Supporting Information for:

Analysis of charge/discharge mechanism of Fe-containing Li_2S positive electrode material and its visualization by computational simulation

Tomonari Takeuchi,[a] Yoyo Hinuma,[*a] Koji Ohara,[b,†1] Hiroyuki Kageyama,[c]
Koji Nakanishi,[c,d,†2] Toshiaki Ohta,[d] So Fujinami,[b,c] Hisao Kiuchi,[c,†3]
and Hikari Sakaebe [a,†4]

[a] *National Institute of Advanced Industrial Science and Technology (AIST)*
Midorigaoka 1-8-31, Ikeda, Osaka 563-8577, Japan
[b] *The Research & Utilization Division, Japan Synchrotron Radiation Research Institute (JASRI), 1-1-1 Kouto, Sayo, Hyogo 679-5198, Japan*
[c] *Office of Society-Academia Collaboration for Innovation, Kyoto University*
Uji, Kyoto 611-0011, Japan
[d] *Synchrotron Radiation Center, Ritsumeikan University*
1-1-1 Noji-Higashi, Kusatsu, Shiga 525-8577, Japan

*to whom correspondence should be addressed

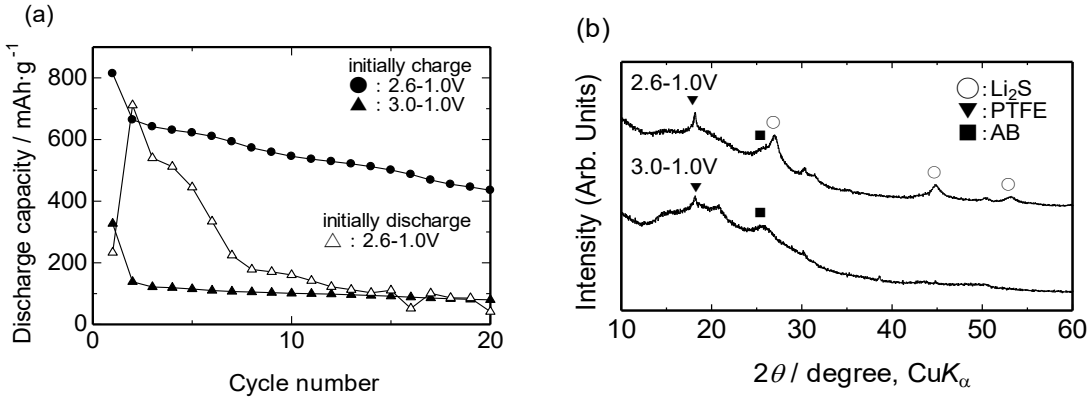

Fig. S1 (a) Cycling performances for the Li_8FeS_5 sample cells at 46.7 $mA \cdot g^{-1}$ (corresponding to 0.04C for $2e^-/Li_2S$) with the voltage range of 3.0-1.0 and 2.6-1.0 V vs. Li^+/Li initially with charging. Data for the cells starting with discharging (2.6-1.0 V) are also shown for reference. (b) XRD patterns for the Li_8FeS_5 samples after 10 cycles with the voltage range of 3.0-1.0 and 2.6-1.0 V vs. Li^+/Li.

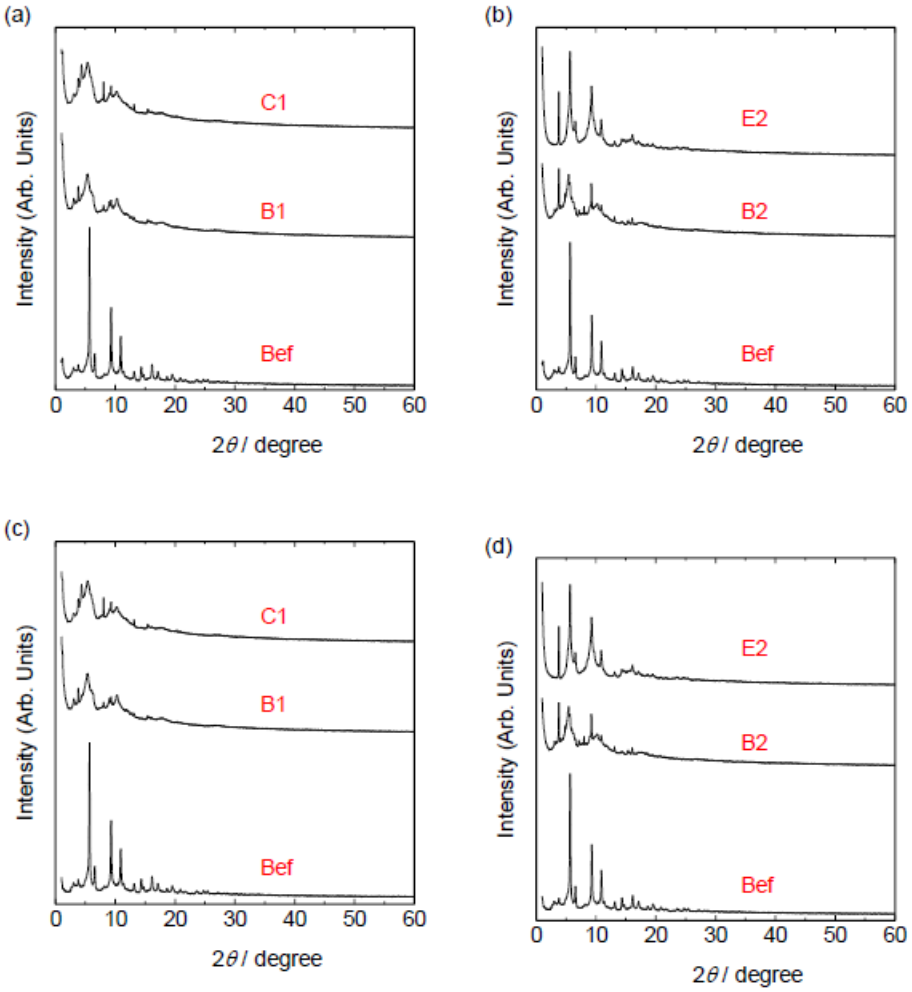

Fig. S2 (a, b) High-energy X-ray total scattering data and (c, d) those after subtracting the background and the contributions from AB and PTFE for the Li_8FeS_5 sample during electrochemical cycling with the voltage range of (a, c) 3.0-1.0 and (b, d) 2.6-1.0 V vs. Li^+/Li. The sample labels such as Bef and B1 correspond to positions in the charge and discharge process shown in Figs. 3(a)(b).

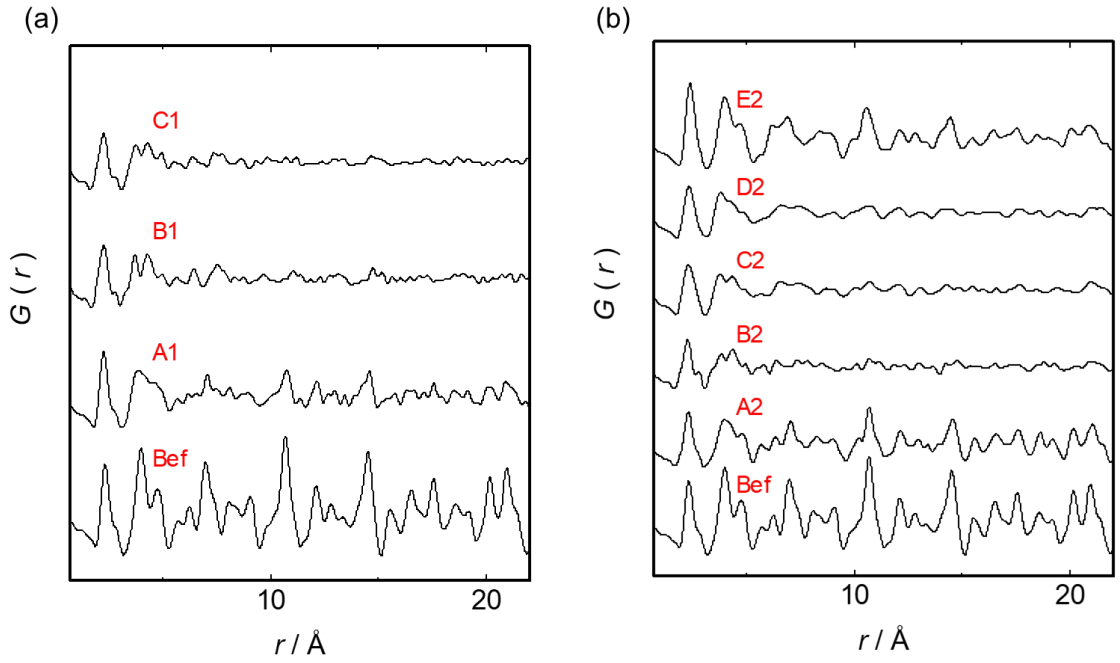

Fig. S3 X-ray radial pair distribution function (PDF) data with a wide range (*ca*. 20 Å) for the Li_8FeS_5 sample during electrochemical cycling with the voltage range of (a) 3.0-1.0 and (b) 2.6-1.0 V vs. Li^+/Li. The sample labels such as Bef and B1 correspond to positions in the charge and discharge process shown in Figs. 3(a)(b).

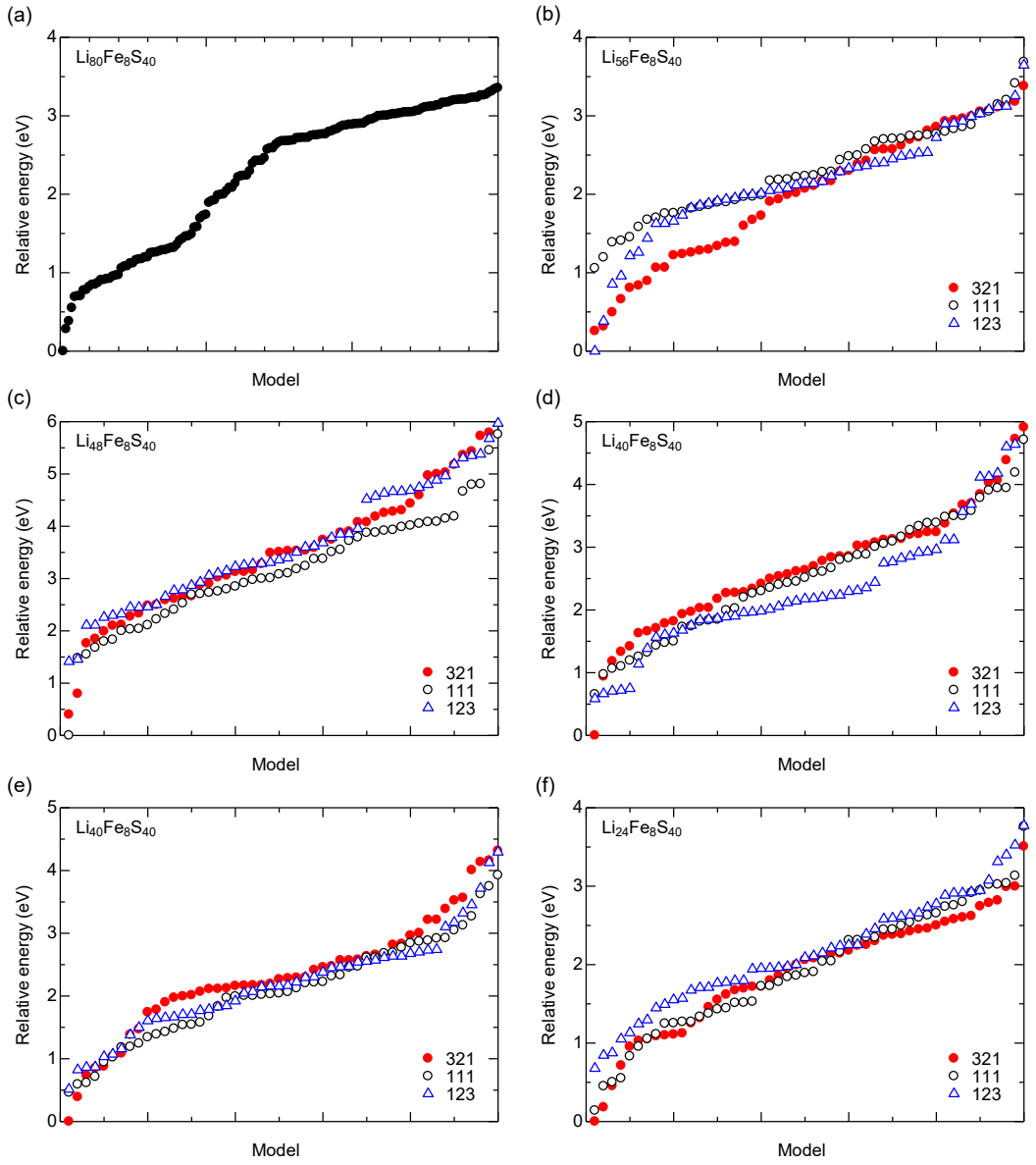

Fig. S4. Relative sorted energies of (a) 150 $Li_{80}Fe_8S_{40}$ models and models each for the 123, 111, and 321 Li extraction methods for (b) $Li_{56}Fe_8S_{40}$, (c) $Li_{48}Fe_8S_{40}$, (d) $Li_{40}Fe_8S_{40}$, (e) $Li_{32}Fe_8S_{40}$, and (f) $Li_{24}Fe_8S_{40}$ (same figure as Fig. 5(b)).

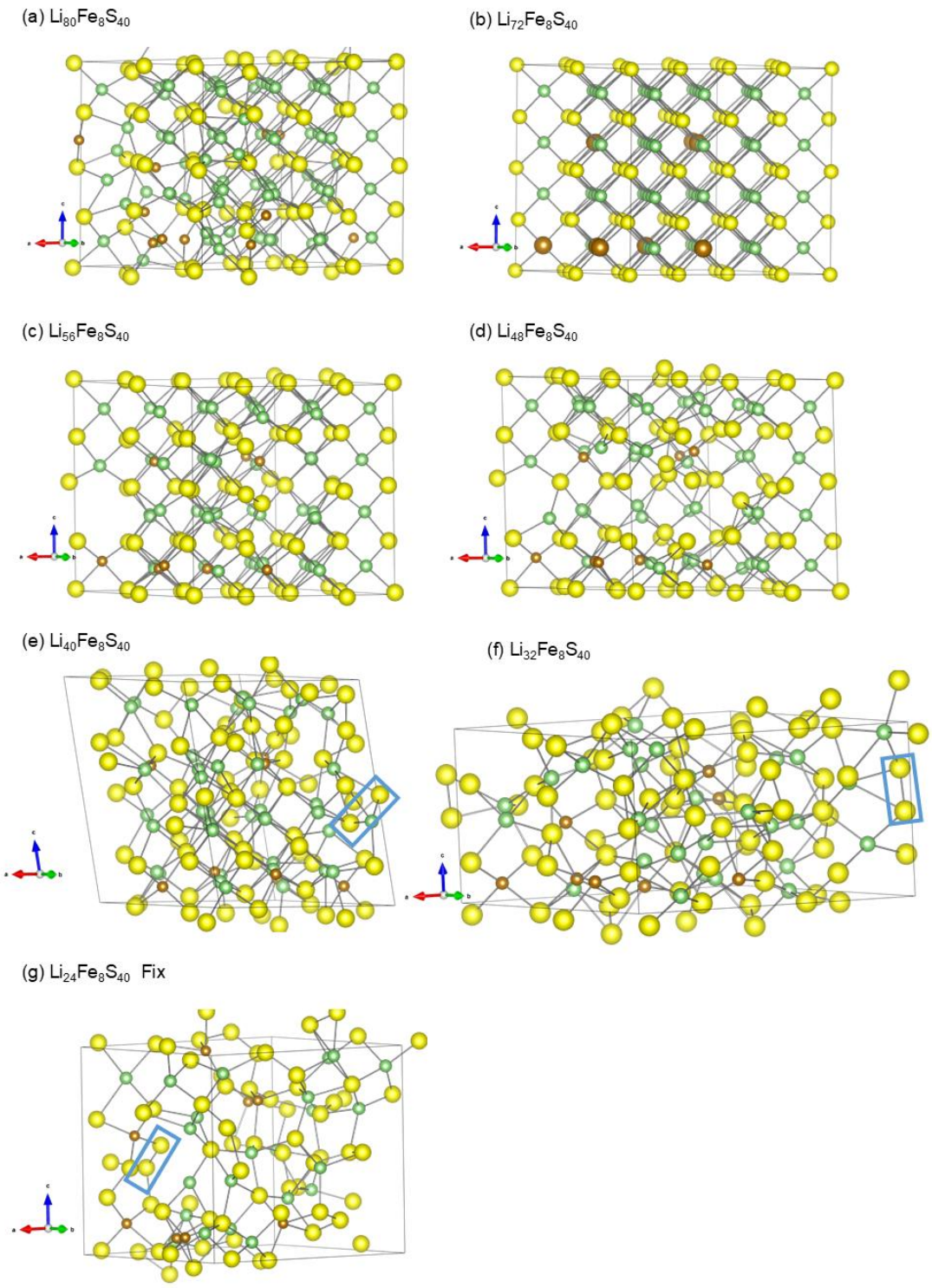

Fig. S5. The lowest energy model of (a) $Li_{80}Fe_8S_{40}$, (b) $Li_{72}Fe_8S_{40}$, (c) $Li_{56}Fe_8S_{40}$, (d) $Li_{48}Fe_8S_{40}$, (e) $Li_{40}Fe_8S_{40}$, (f) $Li_{32}Fe_8S_{40}$, and (g) lattice parameter fixed $Li_{24}Fe_8S_{40}$. Green, brown, and yellow balls correspond to Li, Fe, and S, respectively. S-S bonds with distances less than 2.2Å are shown, and one example is shown in the blue box.

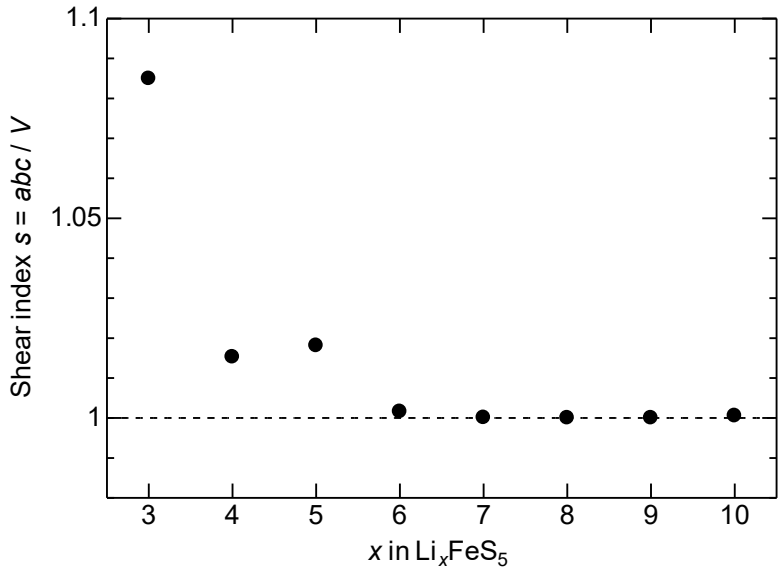

Fig. S6. Shear index $s=abc/V$ of the lowest energy model of Li_xFeS_5. The dashed line is s=1, which is the minimum possible value attained in an exactly orthorhombic lattice.